Frontiers of Information Technology & Electronic Engineering
www.jzus.zju.edu.cn; engineering.cae.cn; www.springerlink.com
ISSN 2095-9184 (print); ISSN 2095-9230 (online)
E-mail: jzus@zju.edu.cn

Event-triggered adaptive tracking control of a class of nonlinear systems with asymmetric time-varying output constraints*

Yitao YANG†‡, Lidong ZHANG

School of Science, Tianjin University of Technology, Tianjin 300384, China

†E-mail: yitaoyangqf@163.com

Received Oct. 8, 2023; Revision accepted Mar. 3, 2024; Crosschecked July 23, 2024

Abstract: This article investigates the event-triggered adaptive neural network (NN) tracking control problem with deferred asymmetric time-varying (DATV) output constraints. To deal with the DATV output constraints, an asymmetric time-varying barrier Lyapunov function (ATBLF) is first built to make the stability analysis and the controller construction simpler. Second, an event-triggered adaptive NN tracking controller is constructed by incorporating an error-shifting function, which ensures that the tracking error converges to an arbitrarily small neighborhood of the origin within a predetermined settling time, consequently optimizing the utilization of network resources. It is theoretically proven that all signals in the closed-loop system are semi-globally uniformly ultimately bounded (SGUUB), while the initial value is outside the constraint boundary. Finally, a single-link robotic arm (SLRA) application example is employed to verify the viability of the acquired control algorithm.

Key words: Adaptive control; Deferred asymmetric time-varying output constraints; Error-shifting function; Event-triggered control

https://doi.org/10.1631/FITEE.2300679 **CLC number:** TP273

1 Introduction

Over the past few decades, the adaptive tracking control problem due to its scientific and technological importance has garnered worldwide interest (Elmokadem et al., 2017; Zhang TP et al., 2017; Guerrero et al., 2020; Qiao and Zhang, 2020). Besides, when uncertainty arises in nonlinear systems, this may introduce serious invisible hazards to engineering systems while they are in use. Plenty of theoretical research in nonlinear systems has been provided in recent years (Xiang et al., 2018; He et al., 2019; Peng et al., 2019; Zhang JJ and Sun, 2020; Qiu et al., 2022). The backstepping technique combined with the neural network (NN) or fuzzy-logic-based approximation theory gave a novel perspective for stabilizing an uncertain nonlinear system (Xiang et al., 2018; Zhang JJ and Sun, 2020).

Most engineering systems are closely related to the output constraint problem, which may degrade the tracking performance of nonlinear systems and even cause system instability because of the constraints of internal factors in the physical devices and also external conditions.

Taking into account the aforementioned issues, several relevant theoretical accomplishments have been reported (Zhang S et al., 2018; Zhao and Chen, 2020; Du et al., 2021; Hu et al., 2021; Wang XJ et al., 2021; Zong et al., 2021; Liu Y et al., 2022; Zhang JM et al., 2022). An innovative solution to managing the issue confronting nonlinear systems was presented by the integration of the adaptive control method with

‡ Corresponding author

* Project supported by the Natural Science Foundation of Tianjin, China (No. 19JCYBJC30700)

ORCID: Yitao YANG, https://orcid.org/0009-0002-7667-6632

© Zhejiang University Press 2024

the NN technique (Zhang S et al., 2018; Du et al., 2021), and the adaptive NN control law was employed to resolve the asymmetric output constraints for the flexible spacecraft (Liu Y et al., 2022). It is important to note that the above results are valid only if the system's initial tracking error fulfills specific needs. This suggests that the selection of design parameters is entirely contingent on the precisely known initial tracking error. However, in engineering applications, where the system may begin with a different initial condition each time, the initial tracking error of the system may vary greatly. For example, the single-link robotic arm (SLRA) system may run from an unconstrained area for a time before moving into a tighter area to accomplish the tracking mission, rendering the above-mentioned management approaches ineffective in certain cases. As a result, when the initial value was outside of the boundaries, a rate function was used to solve the problem (Zhou et al., 2020; Zhao et al., 2022). Although these control schemes had achieved good control performance, they did not account for the restrictions of the deferred asymmetric time-varying (DATV) output constraints, which limited their practical use.

On one hand, time-triggered control (TTC) involves updating the system controller at predetermined time during regular operation. This leads to a significant use of unnecessary computation and communication resources. On the other hand, due to its benefits in minimizing the number of times for data transformation and conserving resources, event-triggered control (ETC) applications have found widespread use in reality (Tabuada, 2007; Heemels et al., 2008; Henningsson et al., 2008). However, the control schemes in Tabuada (2007) and Heemels et al. (2008) were established based upon the assumption that the system satisfied the input-to-state stability (ISS), which was not easy to implement. In Adaldo et al. (2015), the event-triggered pinning control of complex nonlinear network systems was investigated, and the ISS assumption was avoided. Inspired by Adaldo et al. (2015), the idea of the fixed-threshold ETC (FETC) mechanism was used for nonlinear systems (Li ML et al., 2020; Li XM et al., 2020; Ma et al., 2020; Cao et al., 2021). Nevertheless, it is not possible to adjust the event-triggered threshold online in reaction to changes in the control input. Recently, a novel approach to stabilizing uncertain nonlinear systems (Wang AQ et al., 2020; Zhang CH and Yang, 2020) using finite-time control and networked control was developed. The burden of data transmission was decreased by Wang AQ et al. (2019) by using a simultaneous update approach to constructing ETC. Despite extensive research conducted on the ETC for nonlinear systems, the DATV output constraint problem has received less attention. This gap motivated our present research.

The present paper proposes an event-triggered adaptive NN control approach with DATV output constraints, which was motivated by the discussions described above. The major contributions in this field are listed below, comparing them to the existing research:

1. An adaptive NN tracking controller based on the event-triggered mechanism, together with an error-shifting function, is proposed for the SLRA system with uncertain initial values and DATV output constraints, which assures one that all the signals in the closed-loop system are semi-globally uniformly ultimately bounded (SGUUB).

2. In contrast to Zhao and Chen (2020), Du et al. (2021), and Liu Y et al. (2022), the proposed controller combines an error-shifting function not only to attain the predetermined convergence time but also to overcome the barrier Lyapunov function (BLF)'s initial constraint condition. This enhances the practical use of the SLRA.

3. The designed ETC strategy is incorporated into the SLRA system, which not only improves the tracking performance of the SLRA but also progresses the engineering feasibility in the real world. Besides, it reduces the number of times for data transformation from the controller to the actuator and saves communication resources.

2 Problem formulation and preliminaries

2.1 Problem statement

Consider the strict-feedback nonlinear systems:

$$\begin{cases} \dot{x}_i(t)=G_i(\bar{\boldsymbol{x}}_i)x_{i+1}+f_i(\bar{\boldsymbol{x}}_i)+d_i(\bar{\boldsymbol{x}}_i,t), \\ \qquad i=1,2,\ldots,n-1, \\ \dot{x}_n(t)=G_n(\bar{\boldsymbol{x}}_n)u+f_n(\bar{\boldsymbol{x}}_n)+d_n(\bar{\boldsymbol{x}}_n,t), \\ y=x_1(t), \end{cases} \tag{1}$$

subject to DATV output constraints where the system output is unconstrained when $t < T$ and is

restricted with DATV constraint boundaries starting from $t=T$. Here, $\bar{\boldsymbol{x}}_i=[x_1(t),x_2(t),\dots,x_i(t)]^{\mathrm{T}}\in\mathbb{R}^i$ $(i=1,2,\dots,n)$, u, and y are the system state, control input, and system output, respectively. $f_i(\bar{\boldsymbol{x}}_i)$ is an unknown smooth function and $G_i(\bar{\boldsymbol{x}}_i)$ means an unknown continuous control gain function $(i=1,2,\dots,n)$. $d_i(\bar{\boldsymbol{x}}_i,t)$ is the unknown bounded time-varying disturbance.

The control aim is to design an event-triggered adaptive NN controller with the DATV output constraints such that the tracking error $e_1(t)=x_1(t)-y_{\mathrm{d}}(t)$ converges to an arbitrarily small neighborhood of the origin, and the DATV output constraints are not violated after the settling time T.

To achieve the control objective, the following assumptions are employed:

Assumption 1 The following inequality holds:

$$\underline{G}_i\le G_i(\bar{\boldsymbol{x}}_i)\le\bar{G}_i,\ i=1,2,\dots,n, \tag{2}$$

with positive constants $\underline{G}_i$ and $\bar{G}_i$. Without loss of generality, it is assumed that $\underline{G}_i\ge 0$.

Assumption 2 The reference signal $y_{\mathrm{d}}(t)$ is a bounded and continuous function of degree n.

Assumption 3 The following inequality holds:

$$d_i(\bar{\boldsymbol{x}}_i,t)\le\bar{d}_i,\ i=1,2,\dots,n, \tag{3}$$

with unknown constant $\bar{d}_i$.

2.2 Error-shifting function

To overcome the adverse effects of bounded initial values, an error-shifting function is adopted:

$$\varphi(t)=\begin{cases}\dfrac{t^2}{\mathrm{e}^{T-t}(T-t)^2+\epsilon t^2}, & 0\le t<T,\\ \dfrac{1}{\epsilon}, & t\ge T,\end{cases} \tag{4}$$

where T denotes the predetermined settling time and ϵ ($\epsilon\in(0,1]$) is a pre-given positive constant.

Remark 1 The error-shifting function (4) improves the transit and steady-state system performance by modifying T and ϵ. The smaller the T and ϵ, the higher the control cost. Therefore, how to strike a balance between the convergence rate and control cost is crucial.

From Eq. (4), it is readily derived that $\varphi(t)$ has three properties, which are summarized in Lemma 1.

Lemma 1 The constructed error-shifting function $\varphi(t)$ has the following characters:

(1) $\varphi(t)$ is strictly increasing for $t\in[0,T]$ with $\varphi(0)=0$;

(2) $\varphi(t)$ reaches $1/\epsilon$ at $t=T$ and remains stable for $t\ge T$;

(3) $\varphi(t)$ and $\dot{\varphi}(t)$ are continuous and bounded for $t\in[0,\infty)$.

Proof From Eq. (4), when t approaches the left limit of T, we obtain

$$\lim_{t\to T^-}\varphi(t)=\lim_{t\to T^-}\frac{t^2}{\mathrm{e}^{T-t}(T-t)^2+\epsilon t^2}=\frac{1}{\epsilon},$$

$$\lim_{t\to T^+}\varphi(t)=\lim_{t\to T^+}\frac{1}{\epsilon}=\frac{1}{\epsilon}.$$

Hence, we can infer that $\varphi(t)$ is continuous for $t\ge 0$. Next, we prove that $\dot{\varphi}(t)$ exists at the time instant T. From Eq. (4), one has

$$\dot{\varphi}_-(t)=\lim_{t\to T^-}-\frac{\mathrm{e}^{T-t}(T-t)^2}{\epsilon(\mathrm{e}^{T-t}(T-t)^2+\epsilon t^2)}=0,$$

$$\dot{\varphi}_+(t)=\lim_{t\to T^+}\frac{1/\epsilon-1/\epsilon}{t-T}=0.$$

Therefore, the derivative of $\varphi(t)$ is

$$\dot{\varphi}(t)=\begin{cases}\dfrac{t\mathrm{e}^{T-t}(T-t)(-t^2+t(T+2)+2)}{(\mathrm{e}^{T-t}(T-t)^2+\epsilon t^2)^2}, & 0\le t<T,\\ 0, & t\ge T.\end{cases} \tag{5}$$

It is easy to see that $\dot{\varphi}(t)>0$ for $t\in[0,T)$, which indicates that $\varphi(t)$ is strictly increasing for all $t\in[0,T)$. We can learn that $\varphi(0)=0$ and $\varphi(t)$ remains to be $1/\epsilon$ for $t\ge T$. From Eq. (5), $\dot{\varphi}(t)$ is continuous and bounded. This completes the proof.

2.3 Radial basis function neural network (RBFNN)

The RBFNN is used in this subsection to resolve the unknown continuous function $\Psi_{\mathrm{nn}}(\boldsymbol{x})\in\mathbb{R}$:

$$\Psi_{\mathrm{nn}}(\boldsymbol{x})=\boldsymbol{W}^{\mathrm{T}}\boldsymbol{\psi}(\boldsymbol{x}), \tag{6}$$

where $\boldsymbol{x}\in\Omega_{\boldsymbol{x}}\subset\mathbb{R}^p$ is the input vector, $\boldsymbol{W}=[W_1,W_2,\dots,W_q]^{\mathrm{T}}\in\mathbb{R}^q$ denotes the weight, and $\boldsymbol{\psi}(\boldsymbol{x})=[\psi_1(\boldsymbol{x}),\psi_2(\boldsymbol{x}),\dots,\psi_q(\boldsymbol{x})]^{\mathrm{T}}\in\mathbb{R}^q$ is the Gaussian function satisfying

$$\psi_i(\boldsymbol{x})=\exp\left[\frac{-(\boldsymbol{x}-\boldsymbol{\mu}_i)^{\mathrm{T}}(\boldsymbol{x}-\boldsymbol{\mu}_i)}{\tau_i^2}\right],\ i=1,2,\dots,q, \tag{7}$$

with $\boldsymbol{\mu}_i=[\mu_{i1},\mu_{i2},\dots,\mu_{ip}]^{\mathrm{T}}$ denoting the neural cell center and τ_i the Gaussian function width. From the

universal approximation property of RBFNN, one has

$$\Psi_{\mathrm{nn}}(\boldsymbol{x}) = (\boldsymbol{W}^*)^{\mathrm{T}}\boldsymbol{\psi}(\boldsymbol{x}) + \delta(\boldsymbol{x}), \tag{8}$$

where $\boldsymbol{W}^*$ is the ideal constant weight and $\delta(\boldsymbol{x})$ being the approximation error meets

$$|\delta(\boldsymbol{x})| \le \bar{\delta} < \infty,\ \boldsymbol{x} \in \Omega_{\boldsymbol{x}}, \tag{9}$$

with $\bar{\delta}$ being an unknown bounded constant.

2.4 Asymmetric time-varying barrier Lyapunov function (ATBLF)

To overcome the problem of DATV output constraints, the ATBLF is constructed as given below:

$$V_a = \frac{\underline{k}_b(t)\bar{k}_b(t)\nu_1^2(t)}{(\underline{k}_b(t)+\nu_1(t))(\bar{k}_b(t)-\nu_1(t))}, \tag{10}$$

where the upper boundary $\bar{k}_b(t)$ and the lower boundary $\underline{k}_b(t)$ are positive barrier functions respectively, satisfying $-\underline{k}_b(0) < \nu_1(0) < \bar{k}_b(0)$. To realize $-\underline{k}_a(t) < x_1(t) < \bar{k}_a(t)$ after the settling time T, $\underline{k}_b(t)$ and $\bar{k}_b(t)$ should satisfy

$$\underline{k}_b(t) = \underline{k}_a(t) - \underline{y}_{\mathrm{d}},\ \ \bar{k}_b = \bar{k}_a(t) - \bar{y}_{\mathrm{d}}, \tag{11}$$

where $\underline{k}_a(t)$ and $\bar{k}_a(t)$ are positive functions, and $\bar{y}_{\mathrm{d}}$ and $\underline{y}_{\mathrm{d}}$ denote the maximum and minimum values of $y_{\mathrm{d}}(t)$ respectively.

3 Main results

3.1 Controller design and adaptive laws

From Eq. (4), we define

$$e_1(t) = x_1(t) - y_{\mathrm{d}}(t), \tag{12}$$

$$e_i(t) = x_i(t) - \alpha_{i-1},\ i = 2,3,\ldots,n, \tag{13}$$

$$\nu_j(t) = \varphi(t)e_j(t),\ j = 1,2,\ldots,n, \tag{14}$$

where α_i is the virtual control signal.

For $t \in [t_k, t_{k+1})$, the virtual controller and the actual controller are constructed as follows:

$$\begin{aligned}\alpha_1 =& \frac{1}{\underline{G}_1}\big(-k_1e_1(t) - \gamma_1\Lambda_1\nu_1(t)\varphi(t)\hat{\theta}_1\Psi_1 \\ & - \gamma_1\kappa_2^2\Lambda_1e_1(t) + \gamma_1\dot{\varphi}^2(t)\Lambda_1e_1^3(t)\big),\end{aligned} \tag{15}$$

$$\begin{aligned}\alpha_2 =& \frac{1}{\underline{G}_2}\big(-k_2e_2(t) - \gamma_2\nu_2(t)\varphi(t)\hat{\theta}_2\Psi_2 \\ & - \gamma_2\dot{\varphi}^2(t)e_2^3(t)\big),\end{aligned} \tag{16}$$

$$\begin{aligned}\alpha_i =& \frac{1}{\underline{G}_i}\big(-k_ie_i(t) - \gamma_i\nu_i(t)\varphi(t)\hat{\theta}_i\Psi_i - \gamma_i\dot{\varphi}^2(t)e_i^3(t)\big), \\ & i = 3,4,\ldots,n-1,\end{aligned} \tag{17}$$

$$\begin{aligned}\varsigma(t) =& \frac{1}{1-\varepsilon}\left(-\frac{1}{\underline{G}_n}(k_ne_n(t) + \gamma_n\varphi(t)\nu_n(t)\hat{\theta}_n\Psi_n\right. \\ & \left. + \gamma_n\dot{\varphi}^2(t)e_n^3(t)) - \frac{1}{2}\nu_n(t)\varphi(t)\bar{G}_n^2\right),\end{aligned} \tag{18}$$

$$u = \varsigma(t_k), \tag{19}$$

where t_k is the triggering time instant satisfying $t_0 = 0$. k_i and γ_i $(i = 1,2,\ldots,n)$ are design parameters, ε indicates the triggering threshold, and adaptive laws are designed as

$$\dot{\hat{\theta}}_1 = \gamma_1^2\varphi^2(t)\Lambda_1^2\nu_1^2(t)\Psi_1 - \sigma_1\hat{\theta}_1, \tag{20}$$

$$\dot{\hat{\theta}}_2 = \gamma_2^2\varphi^2(t)\nu_2^2(t)\Psi_2 - \sigma_2\hat{\theta}_2, \tag{21}$$

$$\dot{\hat{\theta}}_i = \gamma_i^2\varphi^2(t)\nu_i^2(t)\Psi_i - \sigma_i\hat{\theta}_i,\ i = 3,4,\ldots,n-1, \tag{22}$$

$$\dot{\hat{\theta}}_n = \gamma_n^2\varphi^2(t)\nu_n^2(t)\Psi_n - \sigma_n\hat{\theta}_n, \tag{23}$$

where σ_i is a positive design parameter, and $\hat{\theta}_i$ and θ_i mean the estimate of θ_i and unknown bounded parameter for $i = 1,2,\ldots,n$ with $\hat{\theta}_i = \theta_i - \tilde{\theta}_i$ and $\hat{\theta}_i(0) > 0$ respectively.

Remark 2 It is not difficult to deduce from Eqs. (4), (13), and (14) that any bounded initial value of the error variable is transformed into a new error variable with zero initial value, and the transformed error turns into a new error with adjustable parameter ϵ for $t > T$. As a result, the nonlinear system's tracking performance can be changed online. This feature solves the problem of constrained initial values in traditional methods.

3.2 Event-triggered mechanism

The defined measurement error is

$$e = |\varsigma(t)| - |u|,\ \ t \in [t_k, t_{k+1}), \tag{24}$$

along with the event-triggered condition being constructed as

$$t_{k+1} = \inf\{t > t_k | \hbar(e, \varsigma(t), t) \ge 0\}, \tag{25}$$

where $\hbar(e,\varsigma(t),t) = e - \varepsilon|\varsigma(t)| - m_0$ with $m_0 > 0$ and $0 < \varepsilon < 1$.

While the event occurs at $t = t_k$, the input signal $\varsigma(t_k)$ is sent to the actuator, and then it updates

the current value. When $t \in [t_k, t_{k+1})$, the actuator maintains the current value. Therefore, the data update frequency between the controller and the actuator is effectively reduced by the ETC approach.

Remark 3 For the purpose of avoiding the Zeno behavior, take note that m_0 in Eq. (25) is positive. However, it is not the only one. Other alternatives are available, for instance, $n_0 \mathrm{e}^{-n_1 t}$ with $n_1 > 0$.

3.3 Stability analysis

The design process will be carried out in n steps in this subsection, and the effectiveness of the established controller will be theoretically verified.

Step 1: From system (1) and the definition of tracking error e_1, one has

$$\begin{aligned}\dot{z}_1 =&G_1(\bar{x}_1)x_2 + f_1(\bar{x}_1) + d_1(\bar{x}_1, t) - \dot{y}_{\mathrm{d}}(t)\\ =&G_1(\bar{x}_1)(e_2(t)+\alpha_1)+f_1(\bar{x}_1)\\ &+ d_1(\bar{x}_1, t) - \dot{y}_{\mathrm{d}}(t).\end{aligned} \tag{26}$$

Then, from Eq. (14), we have

$$\begin{aligned}\dot{\nu}_1(t) =&\dot{\varphi}(t)e_1(t) + \varphi(t)G_1(\bar{x}_1)(e_2(t) + \alpha_1)\\ &+ \varphi(t)\big(f_1(\bar{x}_1) + d_1(\bar{x}_1, t) - \dot{y}_{\mathrm{d}}(t)\big)\\ =&\dot{\varphi}(t)e_1(t)+\varphi(t)G_1(\bar{x}_1)\alpha_1+G_1(\bar{x}_1)\nu_2(t)\\ &+ \varphi(t)\big(f_1(\bar{x}_1) + d_1(\bar{x}_1, t) - \dot{y}_{\mathrm{d}}(t)\big).\end{aligned} \tag{27}$$

Consider the Lyapunov function candidate

$$V_1 = V_a + \frac{1}{2\gamma_1}\tilde{\theta}_1^2, \tag{28}$$

where $\gamma_1 > 0$ is the design parameter, and $\tilde{\theta}_1 = \theta_1 - \hat{\theta}_1$ denotes the estimation error. Define $\kappa_2 = (\dot{\underline{k}}_b(t)\bar{k}_b(t)\nu_1(t)(2\underline{k}_b(t)\bar{k}_b(t) + \nu_1(t)(\bar{k}_b(t) - 2\underline{k}_b(t) - \nu_1^2(t))) + \dot{\bar{k}}_b(t)\underline{k}_b(t)\nu_1(t)(2\underline{k}_b(t)\bar{k}_b(t) + \nu_1(t)(2\bar{k}_b(t) - \underline{k}_b(t)) - \nu_1^2(t)))(2\underline{k}_b(t)\bar{k}_b(t)(\bar{k}_b(t)\underline{k}_b(t) + \frac{3}{2}(\bar{k}_b(t) - \underline{k}_b(t)))\nu_1(t))$ and $\Lambda_1 = (2\underline{k}_b(t)\bar{k}_b(t)(\underline{k}_b(t)\bar{k}_b(t) + \frac{3}{2}(\bar{k}_b(t) - \underline{k}_b(t))\nu_1(t)))/((\underline{k}_b(t) + \nu_1(t))(\bar{k}_b(t) - \nu_1(t)))^2$.

Thereby, its derivative is

$$\begin{aligned}\dot{V}_1 =& \Lambda_1\nu_1(t)(\dot{\nu}_1(t) + \kappa_2) - \frac{1}{\gamma_1}\tilde{\theta}_1\dot{\hat{\theta}}_1\\ =& \Lambda_1\nu_1(t)\Big(e_1(t)\dot{\varphi}(t) + \varphi(t)G_1(\bar{x}_1)e_2(t)\\ &+ \varphi(t)G_1(\bar{x}_1)\alpha_1 + \varphi(t)\big((W_1^*)^{\mathrm{T}}\psi_1(\bar{x}_1)\\ &+ \delta_1(\bar{x}_1) - \dot{y}_{\mathrm{d}}(t)\big) + \kappa_2\Big) - \frac{1}{\gamma_1}\tilde{\theta}_1\dot{\hat{\theta}}_1.\end{aligned} \tag{29}$$

Young's inequality combined with Assumption 3 results in

$$\Lambda_1\nu_1(t)\kappa_2 \le \gamma_1\Lambda_1^2\nu_1^2(t)\kappa_2^2 + \frac{1}{4\gamma_1}, \tag{30}$$

$$\Lambda_1\nu_1(t)\varphi(t)\delta_1(\bar{x}_1) \le \gamma_1\varphi^2(t)\Lambda_1^2\nu_1^2(t)\bar{\delta}_1^2 + \frac{1}{4\gamma_1}, \tag{31}$$

$$\Lambda_1\nu_1(t)e_1(t)\dot{\varphi}(t) \le \gamma_1\dot{\varphi}^2(t)\Lambda_1^2\nu_1^2(t)e_1^2(t) + \frac{1}{4\gamma_1}, \tag{32}$$

$$\Lambda_1\nu_1(t)\varphi(t)\dot{y}_{\mathrm{d}}(t) \le \gamma_1\varphi^2(t)\Lambda_1^2\nu_1^2(t)\dot{y}_{\mathrm{d}}^2(t) + \frac{1}{4\gamma_1}, \tag{33}$$

$$\begin{aligned}\Lambda_1\nu_1(t)(W_1^*)^{\mathrm{T}}\varphi(t)\psi_1 \le&\gamma_1\varphi^2(t)\Lambda_1^2\nu_1^2(t)\|W_1^*\|^2\|\psi_1\|^2\\ &+ \frac{1}{4\gamma_1}.\end{aligned} \tag{34}$$

Let $\Xi_1 = \gamma_1\varphi^2(t)\Lambda_1^2\nu_1^2(t)\theta_1\Psi_1$ with

$$\theta_1 = \max\left\{\|W_1^*\|^2, \bar{\delta}_1^2, 1\right\}, \tag{35}$$

$$\Psi_1 = \|\psi_1(\bar{x}_1)\|^2 + 1 + \dot{y}_{\mathrm{d}}^2(t), \tag{36}$$

where Ψ_1 is a calculable function. Then,

$$\begin{aligned}\dot{V}_1 \le&\Lambda_1\nu_1(t)\varphi(t)(G_1(\bar{x}_1)e_2(t)+G_1(\bar{x}_1)\alpha_1)+\gamma_1\varphi^2(t)\\ &\cdot\Lambda_1^2\nu_1^2(t)\theta_1\Psi_1+\gamma_1\Gamma_1^2\nu_1^2(t)(\kappa_2^2 + e_1^2(t)\dot{\varphi}^2(t))\\ &+ \frac{5}{4\gamma_1} - \frac{1}{\gamma_1}\tilde{\theta}_1\dot{\hat{\theta}}_1.\end{aligned} \tag{37}$$

Substituting Eqs. (15) and (20) into inequality (37) leads to

$$\begin{aligned}\dot{V}_1 \le&-\Lambda_1 k_1\nu_1^2(t)+G_1(\bar{x}_1)\Lambda_1\nu_1(t)\nu_2(t)\\ &-\frac{\sigma_1\tilde{\theta}_1^2}{2\gamma_1} + \Delta_1,\end{aligned} \tag{38}$$

where $\Delta_1 = \dfrac{5}{4\gamma_1} + \dfrac{\sigma_1}{2\gamma_1}\theta_1^2$.

Step 2: The derivative of $\nu_2(t)$ is $\dot{\nu}_2(t) = \dot{\varphi}(t)e_2(t) + \varphi(t)(G_2(\bar{\boldsymbol{x}}_2)e_3(t) + G_2(\bar{\boldsymbol{x}}_2)\alpha_2 + f_2(\bar{\boldsymbol{x}}_2) - \dot{\alpha}_1)$. Then, one has

$$\begin{aligned}\nu_2(t)\dot{\nu}_2(t) =&\nu_2(t)\dot{\varphi}(t)e_2(t) + \nu_2(t)\varphi(t)G_2(\bar{\boldsymbol{x}}_2)e_3(t)\\ &+\nu_2(t)\varphi(t)G_2(\bar{\boldsymbol{x}}_2)\alpha_2+\nu_2(t)\varphi(t)\bar{F}_2\end{aligned} \tag{39}$$

with $\bar{F}_2 = f_2(\bar{\boldsymbol{x}}_2) - \dot{\alpha}_1$. Given that $\bar{F}_2$ contains some unknown nonlinear terms, $\bar{F}_2 = (W_2^*)^{\mathrm{T}}\psi_2(\bar{\boldsymbol{x}}_2) + \delta_2(\bar{\boldsymbol{x}}_2)$ is approximated by an RBFNN. Therefore, Eq. (39) is transformed into

$$\begin{aligned}\nu_2(t)\dot{\nu}_2(t) =&\nu_2(t)\dot{\varphi}(t)e_2(t)+\nu_2(t)\varphi(t)G_2(\bar{\boldsymbol{x}}_2)e_3(t)\\ &+ \nu_2(t)\varphi(t)G_2(\bar{\boldsymbol{x}}_2)\alpha_2 + \nu_2(t)\varphi(t)\\ &\cdot\left((W_2^*)^{\mathrm{T}}\psi_2(\bar{\boldsymbol{x}}_2) + \delta_2(\bar{\boldsymbol{x}}_2)\right).\end{aligned} \tag{40}$$

Choose the Lyapunov function V_2 as

$$V_2 = V_1 + \frac{1}{2}\nu_2^2(t) + \frac{1}{2\gamma_2}\tilde{\theta}_2^2. \tag{41}$$

From Eqs. (40) and (41), one has

$$\begin{aligned}\dot{V}_2 \leq & -\Lambda_1 k_1 \nu_1^2(t) - \frac{\sigma_1 \tilde{\theta}_1^2}{2\gamma_1} + G_1(\bar{x}_1)\Lambda_1 \nu_1(t)\nu_2(t) \\ & + \Delta_1 + \nu_2(t)\dot{\varphi}(t)e_2(t) + \nu_2(t)\varphi(t)G_2(\bar{\boldsymbol{x}}_2)e_3(t) \\ & + \nu_2(t)\varphi(t)G_2(\bar{\boldsymbol{x}}_2)\alpha_2 + \nu_2(t)\varphi(t) \\ & \cdot \left((W_2^*)^{\mathrm{T}}\psi_2(\bar{\boldsymbol{x}}_2) + \delta_2(\bar{\boldsymbol{x}}_2)\right).\end{aligned} \tag{42}$$

Similar to inequalities (30)–(34), one has

$$\Xi_2 = \gamma_2 \nu_2^2(t)\varphi^2(t)\theta_2\Psi_2, \tag{43}$$

$$\theta_2 = \max\left\{\|W_2^*\|^2, \bar{\delta}_2^2, \bar{G}_1^2\right\}, \tag{44}$$

$$\Psi_2 = \|\psi_2(\bar{\boldsymbol{x}}_2)\|^2 + 1 + \Gamma_1^2 e_1^2(t), \tag{45}$$

where Ψ_2 is a calculable function. Then,

$$\begin{aligned}\dot{V}_2 \leq & -\Lambda_1 k_1 \nu_1^2(t) - \frac{\sigma_1 \tilde{\theta}_1^2}{2\gamma_1} + \nu_2(t)\varphi(t)(G_2(\bar{\boldsymbol{x}}_2)\alpha_2 \\ & + \gamma_2 \nu_2(t)\varphi(t)\theta_2\Psi_2 + \gamma_2\dot{\varphi}^2(t)e_2^3(t)) + G_2(\bar{\boldsymbol{x}}_2) \\ & \cdot \nu_2(t)\nu_3(t) - \frac{1}{\gamma_2}\tilde{\theta}_2\dot{\hat{\theta}}_2 + \Delta_1 + \frac{1}{\gamma_2}.\end{aligned} \tag{46}$$

Substituting Eqs. (16) and (21) into inequality (46) gives rise to

$$\begin{aligned}\dot{V}_2 \leq & -\Lambda_1 k_1 \nu_1^2(t) - k_2 \nu_2^2(t) - \sum_{j=1}^{2}\frac{\sigma_j \tilde{\theta}_j^2}{2\gamma_j} \\ & + G_2 \nu_2(t)\nu_3(t) + \Delta_2,\end{aligned} \tag{47}$$

where $\Delta_2 = \Delta_1 + \dfrac{1}{\gamma_2} + \dfrac{\sigma_2\theta_2^2}{2\gamma_2}$.

Step i ($i = 3, 4, \ldots, n-1$): Similar to step 2, one has

$$\begin{aligned}\nu_i(t)\dot{\nu}_i(t) = & \nu_i(t)\dot{\varphi}(t)e_i(t) + \nu_i(t)\varphi(t)G_i(\bar{\boldsymbol{x}}_i)e_{i+1}(t) \\ & + \nu_i(t)\varphi(t)\left((W_i^*)^{\mathrm{T}}\psi_i(\bar{\boldsymbol{x}}_i) + \delta_i(\bar{\boldsymbol{x}}_i)\right) \\ & + \nu_i(t)\varphi(t)G_i(\bar{\boldsymbol{x}}_i)\alpha_i,\end{aligned} \tag{48}$$

$$V_i = V_{i-1} + \frac{1}{2}\nu_i^2(t) + \frac{1}{2\gamma_i}\tilde{\theta}_i^2. \tag{49}$$

From expressions (47)–(49), we obtain

$$\begin{aligned}\dot{V}_i \leq & -\Lambda_1 k_1 \nu_1^2(t) - k_2\nu_2^2(t) - \ldots - k_{i-1}\nu_{i-1}^2(t) \\ & - \sum_{j=1}^{i-1}\frac{\sigma_j\tilde{\theta}_j^2}{2\gamma_j} + G_{i-1}(\bar{\boldsymbol{x}}_{i-1})\nu_{i-1}(t)\nu_i(t) + \Delta_{i-1} \\ & + \nu_i(t)\dot{\varphi}(t)e_i(t) + \nu_i(t)\varphi(t)G_i(\bar{\boldsymbol{x}}_i)e_{i+1}(t) \\ & + \nu_i(t)\varphi(t)G_i(\bar{\boldsymbol{x}}_i)\alpha_i + \nu_i(t)\varphi(t)\Big((W_i^*)^{\mathrm{T}} \\ & \cdot \psi_i(\bar{\boldsymbol{x}}_i) + \delta_i(\bar{\boldsymbol{x}}_i)\Big) - \frac{1}{\gamma_i}\tilde{\theta}_i\dot{\hat{\theta}}_i.\end{aligned} \tag{50}$$

Similar to inequalities (30)–(34), one has

$$\Xi_i = \gamma_i \nu_i^2(t)\varphi^2(t)\theta_i\Psi_i, \tag{51}$$

$$\theta_i = \max\left\{\|W_i^*\|^2, \bar{\delta}_i^2, \bar{G}_{i-1}^2\right\}, \tag{52}$$

$$\Psi_i = \|\psi_i(\bar{\boldsymbol{x}}_i)\|^2 + 1 + e_{i-1}^2(t), \tag{53}$$

where Ψ_i is a calculable function, and we obtain

$$\begin{aligned}\dot{V}_i \leq & -\Lambda_1 k_1 \nu_1^2(t) - k_2\nu_2^2(t) - \ldots - k_{i-1}\nu_{i-1}^2(t) \\ & - \sum_{j=1}^{i-1}\frac{\sigma_j\tilde{\theta}_j^2}{2\gamma_j} + \nu_i(t)\varphi(t)(G_i(\bar{\boldsymbol{x}}_i)\alpha_i + \gamma_i\nu_i(t) \\ & \cdot \varphi(t)\theta_i\Psi_i + \gamma_i\dot{\varphi}^2(t)e_i^3(t))G_i(\bar{\boldsymbol{x}}_i)\nu_i(t)\nu_{i+1}(t) \\ & - \frac{1}{\gamma_i}\tilde{\theta}_i\dot{\hat{\theta}}_i + \Delta_{i-1} - \frac{1}{\gamma_i}.\end{aligned} \tag{54}$$

Then, one has

$$\begin{aligned}\dot{V}_i \leq & -\Lambda_1 k_1 \nu_1^2(t) - \sum_{j=2}^{i-1} k_j \nu_j^2(t) - \sum_{j=1}^{n-1}\frac{\sigma_j\tilde{\theta}_j^2}{2\gamma_j} \\ & + G_{i-1}(\bar{\boldsymbol{x}}_{i-1})\nu_{i-1}(t)\nu_i(t) + \Delta_i,\end{aligned} \tag{55}$$

where $\Delta_i = \Delta_{i-1} + \dfrac{1}{\gamma_i} + \dfrac{\sigma_i\theta_i^2}{2\gamma_i}$.

Step n: Take the following Lyapunov function:

$$V_n = V_{n-1} + \frac{1}{2}\nu_n^2(t) + \frac{1}{2\gamma_n}\tilde{\theta}_n^2. \tag{56}$$

Its derivative in $t \in [t_k, t_{k+1})$ satisfies

$$\begin{aligned}\dot{V}_n \leq & -\Lambda_1 k_1 \nu_1^2(t) - \sum_{j=2}^{n-1} k_j \nu_j^2(t) - \sum_{j=1}^{n-1}\frac{\sigma_j\tilde{\theta}_j^2}{2\gamma_j} + \Delta_{n-1} \\ & + \nu_n(t)(\varphi(t)G_n(\bar{\boldsymbol{x}}_n)u + \varphi(t)((W_n^*)^{\mathrm{T}}\psi_n(\bar{\boldsymbol{x}}_n) \\ & + \delta_n(\bar{\boldsymbol{x}}_n)) + \dot{\varphi}(t)e_n(t)) - \frac{1}{\gamma_n}\tilde{\theta}_n\dot{\hat{\theta}}_n \\ \leq & -\Lambda_1 k_1 \nu_1^2(t) - \sum_{j=2}^{n-1} k_j \nu_j^2(t) - \sum_{j=1}^{n-1}\frac{\sigma_j\tilde{\theta}_j^2}{2\gamma_j} + \Delta_{n-1} \\ & + \gamma_n\dot{\varphi}^2(t)\nu_n^2(t)e_n^2(t) + \nu_n(t)\varphi(t)G_n(\bar{\boldsymbol{x}}_n)u \\ & + \gamma_n\nu_n^2(t)\varphi^2(t)\theta_n\Psi_n + \frac{1}{\gamma_n} - \frac{1}{\gamma_n}\tilde{\theta}_n\dot{\hat{\theta}}_n\end{aligned}$$

$$\begin{aligned}
&\le -\Lambda_1 k_1 \nu_1^2(t) - \sum_{j=2}^{n-1} k_j \nu_j^2(t) - \sum_{j=1}^{n-1} \frac{\sigma_j \tilde{\theta}_j^2}{2\gamma_j} + \Delta_{n-1} \\
&\quad + \gamma_n \dot{\varphi}^2(t) \nu_n^2(t) e_n^2(t) + \nu_n(t)\varphi(t) G_n(\bar{\boldsymbol{x}}_n)(\varsigma(t) - e) \\
&\quad + \gamma_n \nu_n^2(t)\varphi^2(t)\theta_n \Psi_n + \frac{1}{\gamma_n} - \frac{1}{\gamma_n}\tilde{\theta}_n \dot{\hat{\theta}}_n \\
&\le -\Lambda_1 k_1 \nu_1^2(t) - \sum_{j=2}^{n-1} k_j \nu_j^2(t) - \sum_{j=1}^{n-1} \frac{\sigma_j \tilde{\theta}_j^2}{2\gamma_j} + \Delta_{n-1} \\
&\quad + \gamma_n \dot{\varphi}^2(t) \nu_n^2(t) e_n^2(t) + \nu_n(t)\varphi(t) G_n(\bar{\boldsymbol{x}}_n)\varsigma(t) \\
&\quad + \nu_n(t)\varphi(t) G_n(\bar{\boldsymbol{x}}_n)(\varepsilon|\varsigma(t)| + m_0) + \gamma_n \\
&\quad \cdot \nu_n^2(t)\varphi^2(t)\theta_n \Psi_n + \frac{1}{\gamma_n} - \frac{1}{\gamma_n}\tilde{\theta}_n \dot{\hat{\theta}}_n. \qquad (57)
\end{aligned}$$

Combining Eq. (18) with Young's inequality leads to

$$\begin{aligned}
\dot{V}_n \le & -\Lambda_1 k_1 \nu_1^2(t) - \sum_{j=2}^{n} k_j \nu_j^2(t) - \sum_{j=1}^{n-1} \frac{\sigma_j \tilde{\theta}_n^2}{2\gamma_j} + \gamma_n \varphi^2(t) \\
& \cdot \nu_n^2(t)\tilde{\theta}_n \Psi_n - \frac{1}{\gamma_n}\tilde{\theta}_n \dot{\hat{\theta}}_n + \Delta_{n-1} + \frac{1}{\gamma_n} + \frac{1}{2} m_0^2. \qquad (58)
\end{aligned}$$

Substituting Eq. (23) into inequality (58) leads to

$$\dot{V}_n \le -\Lambda_1 k_1 \nu_1^2(t) - \sum_{j=2}^{n} k_j \nu_j^2(t) - \sum_{j=1}^{n} \frac{\sigma_j \tilde{\theta}_j^2}{2\gamma_j} + \Delta_n, \qquad (59)$$

where $\Delta_n = \Delta_{n-1} + \dfrac{1}{\gamma_n} + \dfrac{1}{2} m_0^2 + \dfrac{\sigma_n \theta_n^2}{2\gamma_n}$.

The main findings from the discussions above can be summed up as follows:

Theorem 1 For the nonlinear system (1) with DATV output constraints, the virtual control signals (15)–(17), the actual control input signals (18) and (19), and the adaptive laws (20)–(23) are constructed under Assumptions 1–3; then, SGUUB is ensured for all signals of the closed-loop system.

Proof Note that $\tilde{\theta}_j \hat{\theta}_j \le -\dfrac{1}{2}\tilde{\theta}_j^2 + \dfrac{1}{2}\theta_j^2$, $j = 1, 2, \ldots, n$, and $-\underline{k}_b(t) < \nu_1(t) < \bar{k}_b(t)$. We have

$$\begin{aligned}
& \underline{k}_b(t)\bar{k}_b(t) + \frac{3}{2}\left(\bar{k}_b(t) - \underline{k}_b(t)\right)\nu_1(t) \\
& \ge \underline{k}_b(t)\bar{k}_b(t) + \left(\bar{k}_b(t) - \underline{k}_b(t)\right)\nu_1(t) - \nu_1^2(t) \\
& = \left(\underline{k}_b(t) + \nu_1(t)\right)\left(\bar{k}_b(t) - \nu_1(t)\right) \\
& > 0. \qquad (60)
\end{aligned}$$

Due to the fact that $\underline{k}_b(t)$ and $\bar{k}_b(t)$ are positive functions, we have

$$\Lambda_1 \nu_1^2(t) > \frac{2\underline{k}_b(t)\bar{k}_b(t)\nu_1^2(t)}{\left(\left(\underline{k}_b(t) + \nu_1(t)\right)\left(\bar{k}_b(t) - \nu_1(t)\right)\right)^2}. \qquad (61)$$

Then,

$$\begin{aligned}
\dot{V}_n \le & -\Lambda_1 k_1 \nu_1^2(t) - \sum_{j=2}^{n-1} k_j \nu_j^2(t) - \sum_{j=1}^{n-1} \frac{\sigma_j \tilde{\theta}_n^2}{2\gamma_j} - k_n \nu_n^2(t) \\
& - \frac{\sigma_n \tilde{\theta}_n^2}{2\gamma_n} + \Delta_{n-1} + \frac{1}{\gamma_n} + \frac{1}{2} m_0^2 + \frac{\sigma_n \theta_n^2}{2\gamma_n} \\
\le & - k_1 \nu_1^2(t) - \sum_{j=2}^{n-1} k_j \nu_j^2(t) - \sum_{j=1}^{n-1} \frac{\sigma_j \tilde{\theta}_n^2}{2\gamma_j} - k_n \nu_n^2(t) \\
& - \frac{\sigma_n \tilde{\theta}_n^2}{2\gamma_n} + \Delta_{n-1} + \frac{1}{\gamma_n} + \frac{1}{2} m_0^2 + \frac{\sigma_n \theta_n^2}{2\gamma_n} \\
\le & - \iota V_n + \bar{\eta}, \qquad (62)
\end{aligned}$$

where $\iota = \min_{j=1,2,\ldots,n}\{2k_j, \sigma_j\} > 0$ and $\bar{\eta} = \Delta_{n-1} + \dfrac{1}{\gamma_n} + \dfrac{1}{2} m_0^2 + \dfrac{\sigma_n \theta_n^2}{2\gamma_n}$.

Solving inequality (62) leads to

$$0 \le V_n \le \left(V_n(0) - \frac{\bar{\eta}}{\iota}\right) \mathrm{e}^{-\hbar t} + \frac{\bar{\eta}}{\iota}. \qquad (63)$$

Furthermore,

$$\lim_{t \to \infty} \le \sqrt{2\frac{\bar{\eta}}{\iota}}. \qquad (64)$$

Thus, we obtain $V_n \in l_\infty$, which indicates that $\nu_i(t)$ and $\hat{\theta}_i$ $(i = 1, 2, \ldots, n)$ are bounded. This also infers that $\nu_1(t)$ satisfies $\underline{k}_b(t) < \nu_1(t) < \bar{k}_b(t)$ the whole time. From Eqs. (4) and (14), e_1 is bounded for $t \in (0, \infty)$. Since $e_1(t)$ and $y_{\mathrm{d}}(t)$ are bounded, x_1 is bounded. Considering α_1 and $\hat{\theta}_1$, we can learn that $\alpha_1 \in l_\infty$ and $\hat{\theta}_1 \in l_\infty$. From $\nu_2(t) = \varphi(t)e_2(t)$, $x_2(t) = \alpha_1 + e_2(t)$, we can deduce that $x_2(t)$ is bounded. Furthermore, we have that $x_i(t)$ $(i = 3, 4, \ldots, n)$, α_j $(j = 2, 3, \ldots, n-1)$, $\hat{\theta}_i$ $(i = 2, 3, \ldots, n)$, and u are bounded. As a result, all the signals of the closed-loop system are bounded. Therefore, the proof is completed.

Remark 4 It should be noted that in engineering systems, users can alter parameters to enhance control precision and system performance. In this study, increasing k_i, γ_i, or decreasing σ_i can adjust the tracking error. These parameters are theoretically optional. Larger γ_i and smaller σ_i, on the other hand, might lead to larger adaptive parameters, while greater parameter k_i frequently results in extreme system overshoot. Therefore, how to balance the steady-state and transient processes is critical in the actual world.

Remark 5 The output y from inequalities (62)–(64) is relevant to $\bar{\Delta}$ (a bounded constant). In theory, altering the positive parameter m_0 reduces the

system output y. However, a lower m_0 shall increase the times of ETC. Therefore, how to balance tracking performance and ETC times is critical in application.

Next, the Zeno behavior with the designed ETC during regular operation will be analyzed.

Theorem 2 Consider the nonlinear system (1), control inputs (18) and (19), adaptive laws (20)–(23), and event-triggered condition (25), the Zeno behavior is circumvented during the routine operations.

Proof Define

$$\breve{e} = \varsigma(t) - u,\ t \in [t_k, t_{k+1}). \tag{65}$$

Take the derivative of the above equation:

$$\frac{\mathrm{d}}{\mathrm{d}t}|\breve{e}| = \frac{\mathrm{d}}{\mathrm{d}t}\sqrt{\breve{e}^2} \leq |\dot{\breve{e}}| = \left|\frac{\mathrm{d}\varsigma(t)}{\mathrm{d}t}\right|. \tag{66}$$

Since $\varsigma(t)$ is a C^1 function, then $\dfrac{\mathrm{d}\varsigma(t)}{\mathrm{d}t}$ is continuous. From Eq. (18), we know that $\dfrac{\mathrm{d}\varsigma(t)}{\mathrm{d}t}$ is the function of $\nu_i(t), e_i(t)$, and $\hat{\theta}_i$ $(i = 1, 2, \ldots, n)$. Thereby, we find a positive constant M satisfying $\left|\dfrac{\mathrm{d}\varsigma(t)}{\mathrm{d}t}\right| \leq M$. From inequality (66), we have

$$\frac{\mathrm{d}}{\mathrm{d}t}|\breve{e}| \leq M. \tag{67}$$

Combining inequality (67) with comparison lemma yields

$$|\breve{e}| \leq M(t - t_k),\ t \in [t_k, t_{k+1}). \tag{68}$$

From Eq. (24), one has

$$|\breve{e}| \geq ||\varsigma(t)| - |u|| \geq e. \tag{69}$$

Let ζ_k be the lower bound of t_{k+1}–t_k. We obtain

$$\zeta_k = m_0/M > 0. \tag{70}$$

Hence, the proof of Zeno behavior is completed.

Remark 6 This study is predicated on the assumption that cyberattacks and network delays are not discussed. When the following problems arise, they might cause engineering system instability. Therefore, we shall investigate network security-control strategies in the following study.

Remark 7 Unlike the existing TTC and ETC schemes, the relative threshold event-triggered mechanism is designed to replace the fixed one to balance system stability and communication cost. The nonlinear controller requires stronger control effects when the tracking error rapidly changes, and the control input should be updated in time and get a smaller threshold. When the tracking error is close to zero, which means that the control input has not obviously changed, m_0 is chosen to rule out infinite triggering time if $\epsilon|\varsigma(t)|$ is smaller than m_0. Therefore, the proposed control strategy can effectively relieve the SLRA system's controller-to-actuator data transfer burden and advance engineering feasibility in the real world.

Remark 8 Inspired by Gao et al. (2022), the heuristic optimization algorithm can be applied to the motion control and attitude control of the robotic arm. The objective function of multiple optimization indicators, such as tracking accuracy and convergence time, is designed to improve the transient and steady-state responses of the manipulator by optimizing the parameters and input signals of the controller to obtain the optimal solution of the parameters and achieve higher response speed and better motion smoothness. Therefore, how to combine performance constraints with intelligent algorithms is a meaningful topic.

4 Simulation results

We consider the following SLRA from Liu YJ and Tong (2016) to demonstrate the efficacy of the presented approach:

$$M\ddot{p} + \frac{1}{2}mgl\sin p + N\dot{p} = \tau, \tag{71}$$

where the angular rotation, velocity, and acceleration are denoted as p, $\dot{p}$, and $\ddot{p}$, respectively. τ is the control torque. For Eq. (71), Table 1 lists each symbol's physical meaning and parameter values. Defining $x_1(t) = p$, $x_2(t) = \dot{p}$, and $u = \tau$ with the bounded external time-varying disturbances, one has

$$\begin{cases} \dot{x}_1(t) = x_2(t) + d_1(\bar{x}_1, t), \\ \dot{x}_2(t) = -\dfrac{mgl\sin(x_1(t))}{2M} - \dfrac{N}{M}x_2(t) + \dfrac{u}{M} + d_1(\bar{\boldsymbol{x}}_2, t). \end{cases} \tag{72}$$

Choose the appropriate design parameters as follows: $k_1 = 12.8$, $k_2 = 21$, $\gamma_1 = 16$, and $\gamma_2 = 20$. The output constraint boundary functions are set as $\underline{k}_c(t) = 0.25 + 0.02\sin(2t)$ and $\bar{k}_c(t) = 0.25 + \cos(0.5t)$. The desired signal is given as $y_{\mathrm{d}}(t) = 0.21\cos t$, and the external

time-varying disturbances are $d_1(\bar{x}_1,t) = 75 + 18\sin(0.5t)+15\cos(0.2t+\pi/4)$ and $d_2(\bar{\boldsymbol{x}}_2,t) = 86+14\sin(0.2t+\pi/6)$. The RBFNN includes 25 nodes, the centers of which are distributed in a 3D space with $x \in [-4,4]$, $y \in [-4,4]$, and $z \in [-4,4]$; the Gaussian function widths are $\sigma_1 = 4$ and $\sigma_2 = 50$. The ETC parameters are $\varepsilon = 0.0025$ and $m_0 = 0.5$, the settling time is $T = 2$, and the pre-given positive constant is $\epsilon = 0.82$. To verify the effectiveness of the control strategy, simulation results with two initial values $\boldsymbol{x}(0) = [0.24,\ 0.13]^{\mathrm{T}}$ and $\boldsymbol{x}(0) = [0.28,\ 0.13]^{\mathrm{T}}$ are displayed, separately.

Case 1: States are within the constraints before a given time T.

Case 2: States violate the constraints before a given time T.

The simulation results are shown in Figs. 1–6. From these results, the performance analysis and comparison results of Scheme I (the designed method) and Scheme II (Zhao et al., 2022) are shown. In Fig. 1, the curves of x_1 and $y_{\mathrm{d}}(t)$ are displayed with Schemes I and II under cases 1 and 2. It is easy to know from Figs. 1 and 2 that x_1 and $e_1(t)$ do not exceed the boundaries after the preset time T, and we can find that Scheme I realizes smaller tracking errors compared to Scheme II. Fig. 3 gives the control input of TTC, ETC (the designed method), and FETC (Li ML et al., 2020). In Fig. 4, we show the results of triggering instants and inter-event intervals under case 1, and the triggering times are 413 and 446 for ETC and FETC respectively. Similarly, the results under case 2 are shown in Fig. 5, and the triggering times are 421 and 459 for ETC and FETC respectively. Finally, Fig. 6 shows the curves of adaptive laws $\hat{\theta}_i$ $(i = 1, 2)$, displaying that the designed $\hat{\theta}_i$ is bounded.

Table 1 System description

Symbol	Physical meaning	Value
M	Inertia moment	50 kg/m^2
m	Link quality	35 kg
g	Acceleration of gravity	9.8 m/s^2
l	Link length	1 m
N	Damping coefficient	1 N · m · s

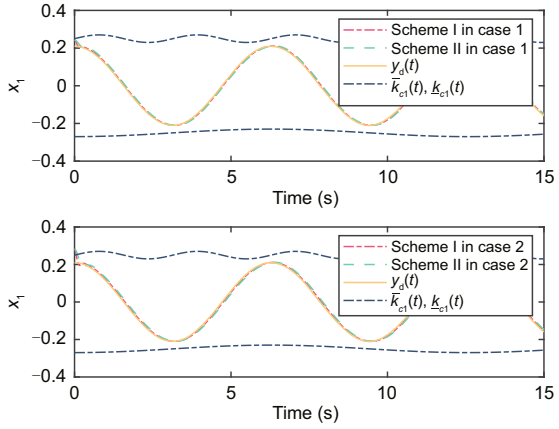

Fig. 1 Curves of x_1 and $y_{\mathrm{d}}(t)$ with Schemes I and II under cases 1 and 2 (Scheme I: the designed method; Scheme II: Zhao et al. (2022)'s method)

5 Conclusions

The problem of event-triggered adaptive NN tracking control has been solved in this study. To address the DATV output constraints, an ATBLF has first been built. In addition, an event-triggered adaptive NN tracking controller has been con-

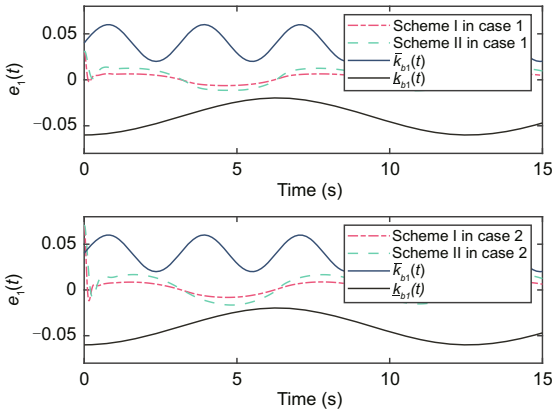

Fig. 2 Curves of the tracking error $e_1(t)$ with Schemes I and II under cases 1 and 2 (Scheme I: the designed method; Scheme II: Zhao et al. (2022)'s method)

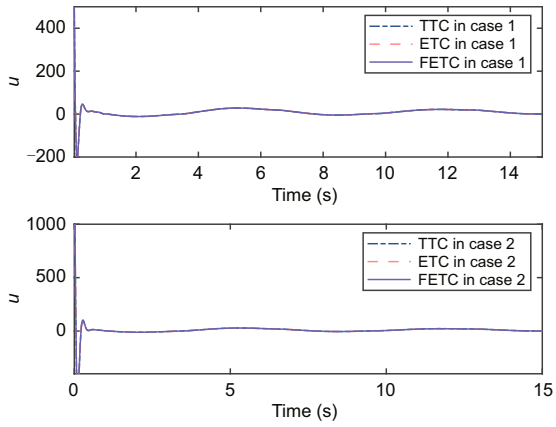

Fig. 3 Curves of the control input under cases 1 and 2 (ETC: event-triggered control; FETC: fixed-threshold ETC; TTC: time-triggered control)

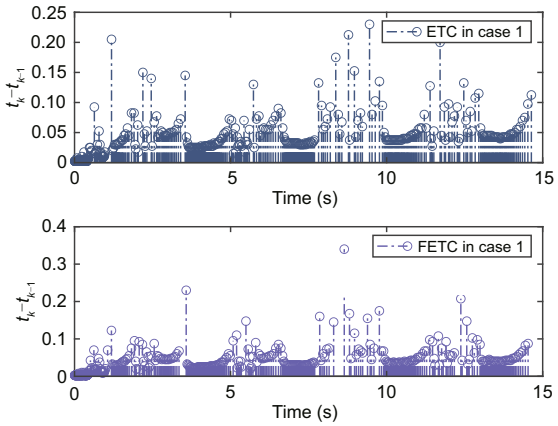

Fig. 4 Triggering instants and inter-event intervals under case 1 (ETC: event-triggered control; FETC: fixed-threshold ETC)

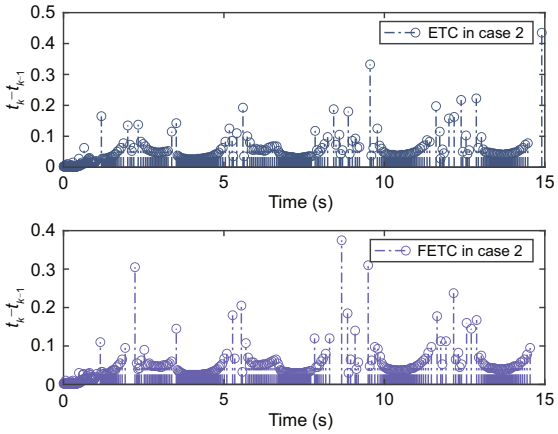

Fig. 5 Triggering instants and inter-event intervals under case 2 (ETC: event-triggered control; FETC: fixed-threshold ETC)

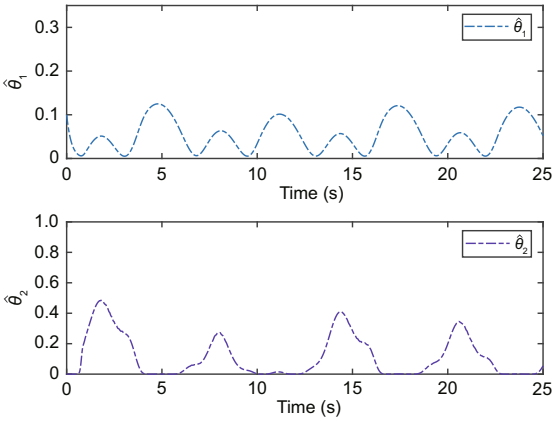

Fig. 6 Curves of $\hat{\theta}_i$ $(i=1,2)$

structed by adding an error-shifting function to increase the usefulness of network resources. It has rigorously been proved mathematically that the initial values can fall beyond the constraint boundary, and that all the signals in the closed-loop system were SGUUB. The viability of the acquired control strategy has been demonstrated using an SLRA application example.

Contributors

Yitao YANG designed the research. Yitao YANG and Lidong ZHANG processed the data. Yitao YANG drafted the paper. Lidong ZHANG helped organize the paper. Yitao YANG and Lidong ZHANG revised and finalized the paper.

Conflict of interest

Both authors declare that they have no conflict of interest.

Data availability

The data are not available.

References

Adaldo A, Alderisio F, Liuzza D, et al., 2015. Event-triggered pinning control of switching networks. *IEEE Trans Contr Netw Syst*, 2(2):204-213. https://doi.org/10.1109/TCNS.2015.2428531

Cao L, Li HY, Dong GW, et al., 2021. Event-triggered control for multiagent systems with sensor faults and input saturation. *IEEE Trans Syst Man Cybern Syst*, 51(6):3855-3866. https://doi.org/10.1109/TSMC.2019.2938216

Du PH, Liang HJ, Zhao SY, et al., 2021. Neural-based decentralized adaptive finite-time control for nonlinear large-scale systems with time-varying output constraints. *IEEE Trans Syst Man Cybern Syst*, 51(5):3136-3147. https://doi.org/10.1109/TSMC.2019.2918351

Elmokadem T, Zribi M, Youcef-Toumi K, 2017. Terminal sliding mode control for the trajectory tracking of underactuated autonomous underwater vehicles. *Ocean Eng*, 129:613-625. https://doi.org/10.1016/j.oceaneng.2016.10.032

Gao HJ, Li ZK, Yu XH, et al., 2022. Hierarchical multi-objective heuristic for PCB assembly optimization in a beam-head surface mounter. *IEEE Trans Cybern*, 52(7):6911-6924. https://doi.org/10.1109/TCYB.2020.3040788

Guerrero J, Torres J, Creuze V, et al., 2020. Adaptive disturbance observer for trajectory tracking control of underwater vehicles. *Ocean Eng*, 200:107080. https://doi.org/10.1016/j.oceaneng.2020.107080

He SD, Dai SL, Luo F, 2019. Asymptotic trajectory tracking control with guaranteed transient behavior for MSV with uncertain dynamics and external disturbances. *IEEE Trans Ind Electron*, 66(5):3712-3720. https://doi.org/10.1109/TIE.2018.2842720

Heemels WPMH, Sandee JH, van den Bosch PPJ, 2008. Analysis of event-driven controllers for linear systems. *Int J Contr*, 81(4):571-590. https://doi.org/10.1080/00207170701506919

Henningsson T, Johannesson E, Cervin A, 2008. Sporadic event-based control of first-order linear stochastic systems. *Automatica*, 44(11):2890-2895. https://doi.org/10.1016/j.automatica.2008.03.026

Hu YB, Geng YH, Wu BL, et al., 2021. Model-free prescribed performance control for spacecraft attitude tracking. *IEEE Trans Contr Syst Technol*, 29(1):165-179. https://doi.org/10.1109/TCST.2020.2968868

Li ML, Li TS, Gao XY, et al., 2020. Adaptive NN event-triggered control for path following of underactuated vessels with finite-time convergence. *Neurocomputing*, 379:203-213. https://doi.org/10.1016/j.neucom.2019.10.044

Li XM, Zhou Q, Li PS, et al., 2020. Event-triggered consensus control for multi-agent systems against false data-injection attacks. *IEEE Trans Cybern*, 50(5):1856-1866. https://doi.org/10.1109/TCYB.2019.2937951

Liu Y, Chen XB, Wu YL, et al., 2022. Adaptive neural network control of a flexible spacecraft subject to input nonlinearity and asymmetric output constraint. *IEEE Trans Neur Netw Learn Syst*, 33(11):6226-6234. https://doi.org/10.1109/TNNLS.2021.3072907

Liu YJ, Tong SC, 2016. Barrier Lyapunov functions-based adaptive control for a class of nonlinear pure-feedback systems with full state constraints. *Automatica*, 64:70-75. https://doi.org/10.1016/j.automatica.2015.10.034

Ma H, Li HY, Lu RQ, et al., 2020. Adaptive event-triggered control for a class of nonlinear systems with periodic disturbances. *Sci China Inform Sci*, 63(5):150212. https://doi.org/10.1007/s11432-019-2680-1

Peng ZH, Wang J, Han QL, 2019. Path-following control of autonomous underwater vehicles subject to velocity and input constraints via neurodynamic optimization. *IEEE Trans Ind Electron*, 66(11):8724-8732. https://doi.org/10.1109/TIE.2018.2885726

Qiao L, Zhang WD, 2020. Trajectory tracking control of AUVs via adaptive fast nonsingular integral terminal sliding mode control. *IEEE Trans Ind Inform*, 16(2):1248-1258. https://doi.org/10.1109/TII.2019.2949007

Qiu JB, Wang T, Sun KK, et al., 2022. Disturbance observer-based adaptive fuzzy control for strict-feedback nonlinear systems with finite-time prescribed performance. *IEEE Trans Fuzzy Syst*, 30(4):1175-1184. https://doi.org/10.1109/TFUZZ.2021.3053327

Tabuada P, 2007. Event-triggered real-time scheduling of stabilizing control tasks. *IEEE Trans Autom Contr*, 52(9):1680-1685. https://doi.org/10.1109/TAC.2007.904277

Wang AQ, Liu L, Qiu JB, et al., 2019. Event-triggered robust adaptive fuzzy control for a class of nonlinear systems. *IEEE Trans Fuzzy Syst*, 27(8):1648-1658. https://doi.org/10.1109/TFUZZ.2018.2886158

Wang AQ, Liu L, Qiu JB, et al., 2020. Finite-time adaptive fuzzy control for nonstrict-feedback nonlinear systems via an event-triggered strategy. *IEEE Trans Fuzzy Syst*, 28(9):2164-2174. https://doi.org/10.1109/TFUZZ.2019.2931228

Wang XJ, Niu B, Song XM, et al., 2021. Neural networks-based adaptive practical preassigned finite-time fault tolerant control for nonlinear time-varying delay systems with full state constraints. *Int J Robust Nonl Contr*, 31(5):1497-1513. https://doi.org/10.1002/rnc.5352

Xiang XB, Yu CY, Lapierre L, et al., 2018. Survey on fuzzy-logic-based guidance and control of marine surface vehicles and underwater vehicles. *Int J Fuzzy Syst*, 20(2):572-586. https://doi.org/10.1007/s40815-017-0401-3

Zhang CH, Yang GH, 2020. Event-triggered global finite-time control for a class of uncertain nonlinear systems. *IEEE Trans Autom Contr*, 65(3):1340-1347. https://doi.org/10.1109/TAC.2019.2928767

Zhang JJ, Sun QM, 2020. Prescribed performance adaptive neural output feedback dynamic surface control for a class of strict-feedback uncertain nonlinear systems with full state constraints and unmodeled dynamics. *Int J Robust Nonl Contr*, 30(2):459-483. https://doi.org/10.1002/rnc.4769

Zhang JM, Niu B, Wang D, et al., 2022. Time-/event-triggered adaptive neural asymptotic tracking control for nonlinear systems with full-state constraints and application to a single-link robot. *IEEE Trans Neur Netw Learn Syst*, 33(11):6690-6700. https://doi.org/10.1109/TNNLS.2021.3082994

Zhang S, Dong YT, Ouyang YC, et al., 2018. Adaptive neural control for robotic manipulators with output constraints and uncertainties. *IEEE Trans Neur Netw Learn Syst*, 29(11):5554-5564. https://doi.org/10.1109/TNNLS.2018.2803827

Zhang TP, Xia MZ, Yi Y, 2017. Adaptive neural dynamic surface control of strict-feedback nonlinear systems with full state constraints and unmodeled dynamics. *Automatica*, 81:232-239. https://doi.org/10.1016/j.automatica.2017.03.033

Zhao K, Chen JW, 2020. Adaptive neural quantized control of MIMO nonlinear systems under actuation faults and time-varying output constraints. *IEEE Trans Neur Netw Learn Syst*, 31(9):3471-3481. https://doi.org/10.1109/TNNLS.2019.2944690

Zhao K, Chen L, Chen CLP, 2022. Event-based adaptive neural control of nonlinear systems with deferred constraint. *IEEE Trans Syst Man Cybern Syst*, 52(10):6273-6282. https://doi.org/10.1109/TSMC.2022.3143359

Zhou SY, Song YD, Luo XS, 2020. Fault-tolerant tracking control with guaranteed performance for nonlinearly parameterized systems under uncertain initial conditions. *J Franklin Inst*, 357(11):6805-6823. https://doi.org/10.1016/j.jfranklin.2020.04.057

Zong GD, Sun HB, Nguang SK, 2021. Decentralized adaptive neuro-output feedback saturated control for INS and its application to AUV. *IEEE Trans Neur Netw Learn Syst*, 32(12):5492-5501. https://doi.org/10.1109/TNNLS.2021.3050992